Development 139, 1417-1426 (2012) doi:10.1242/dev.073239

Cell movements of the deep layer of non-neural ectoderm underlie complete neural tube closure in *Xenopus*

Hitoshi Morita[1], Hiroko Kajiura-Kobayashi[2], Chiyo Takagi[1], Takamasa S. Yamamoto[1], Shigenori Nonaka[2,3] and Naoto Ueno[1,3,*]

SUMMARY

In developing vertebrates, the neural tube forms from a sheet of neural ectoderm by complex cell movements and morphogenesis. Convergent extension movements and the apical constriction along with apical-basal elongation of cells in the neural ectoderm are thought to be essential for the neural tube closure (NTC) process. In addition, it is known that non-neural ectoderm also plays a crucial role in this process, as the neural tube fails to close in the absence of this tissue in chick and axolotl. However, the cellular and molecular mechanisms by which it functions in NTC are as yet unclear. We demonstrate here that the non-neural superficial epithelium moves in the direction of tensile forces applied along the dorsal-ventral axis during NTC. We found that this force is partly attributable to the deep layer of non-neural ectoderm cells, which moved collectively towards the dorsal midline along with the superficial layer. Moreover, inhibition of this movement by deleting integrin β1 function resulted in incomplete NTC. Furthermore, we demonstrated that other proposed mechanisms, such as oriented cell division, cell rearrangement and cell-shape changes have no or only minor roles in the non-neural movement. This study is the first to demonstrate dorsally oriented deep-cell migration in non-neural ectoderm, and suggests that a global reorganization of embryo tissues is involved in NTC.

KEY WORDS: Neural tube closure, Non-neural ectoderm, Deep layer cell, *Xenopus*

INTRODUCTION

Neural tube closure (NTC) is a characteristic dynamic event in vertebrate development, through which the anlage of the future central nervous system is established as a tubular structure. The neural tube (NT) forms as follows. Dorsal ectodermal tissue thickens and becomes the neural plate, the lateral edges of the neural plate rise as neural folds and the center of the plate becomes concave, creating the neural groove; the neural folds continue to rise and bend towards the midline, finally fusing at the dorsal midline (Davidson and Keller, 1999; Colas and Schoenwolf, 2001). It has been known that NTC requires both neural ectoderm, which lies in the dorsal side, and non-neural ectoderm (or epidermal ectoderm), which covers most of the outer surface of embryo (Jacobson and Moury, 1995; Hackett et al., 1997; Smith and Schoenwolf, 1997; Colas and Schoenwolf, 2001; Wallingford, 2005).

The driving forces enabling the NT to close are attributed to both intrinsic and extrinsic forces (Smith and Schoenwolf, 1997; Colas and Schoenwolf, 2001). The intrinsic forces include cell-shape changes, cell rearrangement, and cell division within the neural ectoderm, and they are responsible for remodeling, furrowing and rostrocaudal elongation of this tissue. Neural ectoderm cells undergo convergent extension and apical constriction: the former occurs with the cell-shape change to a bipolar morphology and cell rearrangement; the latter involves a morphological change in the cells to form a wedge shape (Burnside, 1971; Keller et al., 1992). The molecular and cellular mechanisms that regulate convergent extension and apical constriction have been extensively studied (Wallingford and Harland, 2002; Lee et al., 2007; Nishimura and Takeichi, 2008; Roffers-Agarwal et al., 2008; Rolo et al., 2009; Lee and Harland, 2010; Morita et al., 2010; Suzuki et al., 2010).

Unlike the intrinsic forces, the cellular and molecular mechanisms underlying the extrinsic forces are poorly understood. They are mainly generated by the medially directed expansion of non-neural ectoderm, which is required for neural fold formation and neural groove closure (Smith and Schoenwolf, 1997), and were thought to result from cell division, cell-shape changes, cell rearrangement or a combination in the non-neural ectoderm (Burnside, 1973; Smith and Schoenwolf, 1997). Cell division in the non-neural ectoderm of the chicken embryo occurs in the plane perpendicular to the mediolateral axis (Sausedo et al., 1997) and could contribute to mediolateral expansion. Cell-shape changes in the non-neural ectoderm is observed in chick and amphibians, with a decrease in the height and a increase in surface area of these cells (Schoenwolf and Alvarez, 1991), and could contribute to the expansion of this tissue. In the chicken embryo, cell rearrangement in the form of convergent extension occurs in the non-neural ectoderm, and leads to the medial expansion of this tissue (Schoenwolf and Alvarez, 1991), presumably contributing to NTC. Although these cellular changes have been reported, their requirement for non-neural tissue expansion and NTC to occur is only presumptive. Furthermore, how the expansion of non-neural ectoderm is driven is still unclear.

Here, we have analyzed the contribution of non-neural ectoderm to NTC using *Xenopus laevis*, in which neurulation occurs in a similar manner to that of chick and mouse. To learn about the motive force(s) for non-neural cell movement in *Xenopus* neurulation, we examined the candidate factors mentioned above,

[1]Division of Morphogenesis, National Institute for Basic Biology, Nishigonaka 38, Myodaiji, Okazaki, Aichi 444-8585, Japan. [2]Laboratory for Spatiotemporal Regulations, National Institute for Basic Biology, Nishigonaka 38, Myodaiji, Okazaki, Aichi 444-8585, Japan. [3]Department of Basic Biology, School of Life Science, The Graduate University for Advanced Studies (SOKENDAI), Shonan Village, Hayama, Kanagawa 240-0193, Japan.

*Author for correspondence (nueno@nibb.ac.jp)

Accepted 6 February 2012

namely, cell division, cell-shape changes and cell rearrangement, and explored the involvement of physical forces in the oriented cell movement.

MATERIALS AND METHODS

DNA constructs, mRNA and morpholino oligonucleotide

Constructs for membrane-targeted green fluorescent protein (memGFP), enhanced GFP (memEGFP) and red fluorescent protein (memRFP) were generated by fusing the farnesylation signal of c-Ha-Ras to the C terminus of GFP, EGFP and RFP, respectively. *Xenopus laevis* integrin-β1B was obtained from clone number XL412o04ex [XDB3 database, National Institute for Basic Biology (NIBB)]. A rescue construct of integrin-β1B (integrin-β1-res) was generated by changing the nucleotides (indicated by lower letters) of *integrin-β1B* by PCR: (–4) 5′-attaATGGCtaGgTAcCCcGTcTTC-3′ (+21). Venus-tagged integrin-β1 constructs were generated by fusing Venus (Nagai et al., 2002) to their C terminus.

The mRNAs were synthesized using mMESSAGE mMACHINE SP6 (Ambion) and purified on a NICK column (17-0855-02; GE Healthcare). Antisense morpholino oligonucleotide (MO; Gene Tools) against integrin-β1 consisted of the following sequence: 5′-GAATACTGGATAACGGGCCATCTTA-3′. Nec2-MO, Ecad-MO and control MO were as described previously (Nandadasa et al., 2009; Morita et al., 2010).

Embryo culture, transgenesis and microinjection

Xenopus laevis embryos were obtained by standard methods (Morita et al., 2010). A memEGFP-transgenic strain of *Xenopus laevis* was generated as described previously (Kroll and Amaya, 1996; Amaya and Kroll, 1999) with one modification: we prepared sperm nuclei using digitonin. Injections were made at the eight-cell stage into the animal-ventral blastomeres in all experiments except for the laser-ablation experiment. Embryos were staged according to Nieuwkoop and Faber (Nieuwkoop and Faber, 1994). The animals were handled in accordance with the guidelines of the Center for Experimental Animals of the National Institutes of Natural Sciences at Okazaki.

Dorsal explant experiment

The dorsal region of early neurula embryos (stage 13) was excised in Steinberg's solution containing 0.1% bovine serum albumin (BSA) and 100 mg l^{-1} kanamycin. Large explants included all the neural ectoderm and non-neural ectoderm, which correspond to nearly the entire dorsal half of the embryo. Small explants consisted of about two-thirds of the neural ectoderm, with the midline at the center of the explant. Explants were cultured in the same solution under a coverslip. For mesendoderm-free explants, mesendoderm of the large explants were removed in modified DFA solution (Sater et al., 1993). The explants were cultured on a dish coated with 20 μg ml^{-1} fibronectin (FN) (F-1141; Sigma) in Steinberg's solution. At the late neurula stage (stage 20), the explants were fixed in MEMFA [0.1 M MOPS (pH 7.4), 2 mM EGTA, 1 mM $MgSO_4$, 3.7% formalin] for 30 minutes at room temperature and used for further analyses.

Immunohistochemistry

The fixation methods used depended on the primary antibodies to be used for immunohistochemistry. For anti-phospho-histone H3 (pHH3), whole embryos were fixed in 4% paraformaldehyde in PBS for 45 minutes at room temperature. For anti-ZO-1 and -E-cadherin, embryos were fixed in Dent's fixative (Dent et al., 1989). For anti-integrin-β1 and -FN, embryos were fixed in 3.7% formaldehyde in PBS for 45 minutes at room temperature. For other primary antibodies, embryos were fixed in MEMFA for 1-1.5 hours at room temperature. Procedures after fixation were as described previously (Morita et al., 2010).

In situ hybridization and RT-PCR

In situ hybridization was performed as described previously (Harland, 1991; Goda et al., 2009; Suzuki et al., 2010). RT-PCR analysis was performed as described previously (Chung et al., 2005). Primers for the following molecules were used: *NCAM* (Suzuki et al., 1995); *epidermal keratin I* (Suzuki et al., 2010); *MyoDa* (Rupp and Weintraub, 1991); *ODC* (Agius et al., 2000); *sox2*, forward 5′-AGAACCCCAAGATGCACAAC-3′ and reverse 5′-GGACATGCTGTAGGTAGGCGA-3′; *sox17*, forward 5′-CCGGGTAGGAACTGTACAAC-3′ and reverse 5′-TAACCCAGGCTGAAGTTCTC-3′.

Hydroxyurea and aphidicolin (HUA) treatment

HUA treatment was performed as described previously (Harris and Hartenstein, 1991; Hardcastle and Papalopulu, 2000) with some modifications. In brief, the vitelline membrane of early neurula embryos (stage 12-13) was removed in 0.1× MMR (Ubbels et al., 1983). The embryos were cultured in 0.1× MMR- or HUA [20 mM hydroxyurea (H8627; Sigma), 150 mM aphidicolin (A0781; Sigma) and 0.1× MMR] until the desired stages.

Digital scanned laser light sheet fluorescence microscopy (DSLM)

The DSLM system at NIBB was based on the system at the European Molecular Biology Laboratory (EMBL), Heidelberg (Keller et al., 2008). The illumination and detection systems used in this study were an argon krypton laser (488 nm; 643-RYB-A01; Melles Griot, NM, USA), a Plan-Apochromat 5×/0.16 illumination objective lens (Zeiss), a Fluar 5×/0.25 detection objective (Zeiss) and a digital CCD camera (ORCA-AG; Hamamatsu Photonics).

Early neurula embryos (stage 12-13) of the memEGFP-transgenic strain were embedded in 1.2% low-melting-temperature agarose (5517UB; BRL, MD, USA) in a glass capillary (100 μl type; Brand, Wertheim, Germany) at the desired orientation. The capillary was positioned on the DSLM stage system with the sample agarose kept in a sample chamber filled with Steinberg's solution, using a syringe (Brand). Time-lapse images of the memEGFP fluorescence from at least in two angles [dorsal (0°) and one lateral (90°) side] were obtained by rotating the embryos. We also observed the embryos from four angles (0°, 90°, 180° and 270°), and confirmed that the cell movements on both lateral sides were essentially the same (data not shown). Images of 1344 × 1024 pixels were obtained as *z*-series for 5-7 hours at 5-minute intervals with temperature adjusted to 25-27°C. After time-lapse imaging, the embryos were removed from the agarose and incubated in Steinberg's solution and most of them developed normally at least until the tadpole stage (~stage 45).

Laser ablation

For the laser ablation experiment, 400 pg memGFP was injected into four animal blastomeres at the eight-cell stage. Just before imaging, they were embedded in 15 μl of 1.2% low-melting-temperature agarose on a plastic dish, which was then filled with Steinberg's solution. To observe and cut a relatively flat area of the surface, the embryo was set on the microscope sample stage so that its lateralmost aspect was at the center of the confocal image. A fluorescent image was obtained using an FV1000 (Olympus) with a LUMPlan FLN 40×/0.8 water-immersion objective and LD laser (473 nm), at 512 × 512 pixels. Laser ablation was performed using a UV laser (349 nm; Explore 349; Spectra Physics) at 60% power with a 12.5% ND filter. Following the centerline of the image, the surface of the embryo was cut for about 170 μm vertically or horizontally, over a duration of 500 mseconds. The ablation procedure was automated using the Time Controller mode of the FluoView software (Olympus). Fluorescent images of memGFP were obtained just before and after (1.5 seconds) the ablation.

Image acquisition of fixed samples and deep cells

Fluorescent images of deep-layer cells in the non-neural ectoderm and of fixed samples were obtained as previously described (Morita et al., 2010). To observe the deep cells, 200 pg of memGFP mRNA was injected, and the embryos were examined from the early to late neurula stages (stage 13-20) by being embedded in 1.2% low-melting-temperature agarose on a glass-base dish (3910-035; AGC, Tokyo, Japan). Deep cell observation was performed using a low laser power (<10%) to avoid phototoxicity, at 2-minute intervals, at around 25°C.

Image processing and analyses

DSLM time-lapse images were processed using ImageJ (v1.43r; NIH) and Matlab (R2010a; The MathWorks). Maximum *z*-series projections were generated for each time point. The cell displacement in the projected images was traced using ImageJ's 'Manual Tracking' plug-in, which gives

x- and *y*-coordinates. To obtain *z*-coordinates of the embryo image using Matlab, the *x*-*y* images of every fifth *z*-slice were outlined by image processing to make a 'contour map' of the embryo, then interpolated to assign *z*-coordinate values to all the pixels of the *x*-*y* image. This three-dimensional representation of the surface of the embryo was then used to determine the *z*-value of each tracking point and to calculate the precise velocity of the tracking data. The relative velocities in dorsal, medial and ventral regions were measured by equally dividing the lateral view of the DSLM images along the AP axis. The aspect ratio of the non-neural cells was determined for a relatively flat area in fluorescent images by fitting an ellipse to each cell. The angle of the major axis was represented as if it were on the left side of the embryo for purposes of comparison.

Laser ablation images were processed to detect and linearize the cell membrane into one pixel, merge images obtained before and after incision and measure the displacement of cell vertices. To avoid confounds from the cells being at different distances from the ablation line, the distance between the cell vertices and the ablation line was calculated as a weighted mean in which the more distant the center of two vertices was from the ablation line, the greater the factor (from zero to one) that was used to multiply the measured distance of each vertex.

Deep cell movement was tracked using 'Manual Tracking'. The relative distance was measured for pairs of cells consisting of a superficial cell and an adjacent deep cell that was within a one-cell distance (about <30 μm) from the periphery of the superficial cell. Statistical analyses were performed with the paired Student's *t*-test.

Western blot

Western blot for the exogenous integrin-β1-venus was performed as described previously (Morita et al., 2010). For the endogenous integrin-β1, 10 pmol of Itgβ1-MO was injected along with 100 pg of *venus* mRNA. At the early neurula stage, ventral Venus-positive tissues were dissected from 30 of the injected embryos in homogenization buffer [83 mM NaCl, 1 mM $MgCl_2$, 10 mM HEPES (pH 7.9), 0.5 mM PMSF, 10 μg ml^{-1} leupeptin] (Bayaa et al., 2000). Subsequently, the mesoderm and endoderm were removed. The samples were then subjected to western blot as described previously (Bayaa et al., 2000).

Superficial layer transplantation

To label the non-neural ectoderm with fluorescent proteins, eight-cell stage embryos were injected with *memGFP* mRNA and Itgβ1-MO or *memRFP* mRNA alone into the animal-ventral blastomeres. At the early neurula stage, the ventral half of the superficial layer were removed in Ca^{2+}, Mg^{2+}-free MBS [88 mM NaCl, 1 mM KCl, 5 mM HEPES (pH 7.8), 2.5 mM $NaHCO_3$] and transplanted by swapping the host embryos in Steinberg's solution containing 0.1% BSA, and cultured in the same solution.

Antibodies

For immunohistochemistry, the following antibodies were used at the indicated dilutions. The primary antibodies were rabbit anti-pHH3 (1:200; 06-570; Upstate), rat anti-ZO-1 (1:200; AB 01003; Sanko Junyaku), mouse anti-E-cadherin (1:200; 5D3; DSHB), rabbit anti-GFP (1:500; 598; MBL), mouse anti-RFP (1:200; M155-3; MBL), mouse anti-integrin-β1 (1:100; 8C8; DSHB), mouse anti-fibronectin (1:100; MT4; DSHB) and rabbit anti-active caspase 3 (1:400; 559565; BD Biosciences). The secondary antibodies were Alexa Fluor 488 goat anti-rabbit IgG, Alexa Fluor 555 goat anti-rabbit IgG (Molecular Probes), Cy5-conjugated goat anti-rabbit IgG, Cy5-conjugated goat anti-mouse IgG and Cy5-conjugated donkey anti-rat IgG (Jackson ImmunoResearch), used at 1:500. For filamentous actin (F-actin) staining, 4 U ml^{-1} Alexa Fluor 546 phalloidin (A22283; Molecular Probes) was added to the secondary antibodies. For nuclear staining, 50 nM SYTOX Green (S-7020; Molecular Probes) was added to the secondary antibodies.

For western blots, the following antibodies were used at the indicated dilutions. The primary antibodies were rabbit anti-GFP (1:2000; A11122; Molecular Probes), mouse anti-α-tubulin (1:2000; DM 1A; Sigma), mouse anti-integrin-β1 (1:1000; 8C8) and mouse anti-actin (1:400; ACTN05; Thermo). The secondary antibodies were sheep anti-mouse IgG HRP-conjugated (1:10,000; NA9310; GE Healthcare) and donkey anti-rabbit IgG HRP-conjugated (1:10,000; NA9340; GE Healthcare).

RESULTS

Non-neural ectoderm is required for complete NTC

To understand the cellular basis of NTC, we first tested requirement of non-neural ectoderm in *Xenopus* NTC with explant experiment (see Materials and methods). The large explants, consisting of neural and non-neural ectoderm, mostly achieved NTC (closed NT, *n*=16/23; supplementary material Fig. S1A,C,D). By contrast, the small explants that included only the neural ectoderm failed to close the NT (*n*=2/19; supplementary material Fig. S1B,E,F), even though they exhibited typical apical constriction and cell elongation as observed in intact embryos (supplementary material Fig. S1F, inset) (Lee et al., 2007; Rolo et al., 2009; Morita et al., 2010; Suzuki et al., 2010). Expression of marker genes for neural and non-neural ectoderm was confirmed by in situ hybridization (supplementary material Fig. S1G-R). We repeated this experiments without mesendoderm to test its involvement in NTC (supplementary material Fig. S1W). When intact siblings closed the NTs, most mesendoderm-free explants had also closed their NT (*n*=27/36; supplementary material Fig. S1S,T). Cross-sections of these explants showed a completely closed tubular structure at the midline (supplementary material Fig. S1U,V), consistent with previous reports using chick and axolotl (Alvarez and Schoenwolf, 1992; Jacobson and Moury, 1995; Hackett et al., 1997), supporting the idea that non-neural ectoderm contributes significantly to NTC.

Cell division is not an essential driving force for *Xenopus* NTC

We next examined how the non-neural ectoderm contributes to NTC. As the oriented cell division was introduced as a possible driving force in chick NTC (Sausedo et al., 1997), we tested this possibility with DNA synthesis inhibitors, hydroxyurea and aphidicolin (HUA; supplementary material Fig. S2A-E) (Harris and Hartenstein, 1991). When soaked in HUA solution from the early neurula stage, the external morphology of neurula embryo was indistinguishable from that of untreated ones during NTC (closed NT, *n*=35/37; supplementary material Fig. S2F,G and Movies 1 and 2), consistent with a previous study (Harris and Hartenstein, 1991). Cross-sections showed that the HUA-treated embryos reached complete NTC (supplementary material Fig. S2H,I), suggesting that cell division is dispensable for *Xenopus* NTC.

Global cell movements of non-neural ectoderm and cell-shape change suggest the presence of force

We speculated that, instead of proliferation, dynamic cell movement by the non-neural ectoderm during embryogenesis might contribute to the completion of NTC. We therefore analyzed the global ectoderm cell movement by DSLM (Keller et al., 2008). Using DSLM and a memEGFP transgenic strain of *Xenopus laevis*, which expresses memEGFP in all tissues, we were able to observe the cellular dynamics of NTC in a whole embryo (Fig. 1A-D). We found that most of the non-neural ectoderm cells moved towards the dorsal side (supplementary material Movies 3, 4), which is consistent with previous observations in amphibian embryos (Keller, 1976; Veldhuis et al., 2005). We also found that cells in the medial region of the anteroposterior (AP) axis moved faster than those at the AP ends (Fig. 1E) and that the cells located in the region close to the dorsal side moved faster than those in more ventral side (Fig. 1F), indicating velocity gradients along both dorsoventral (DV) and AP axes. Importantly, most of these trajectories were basically in the

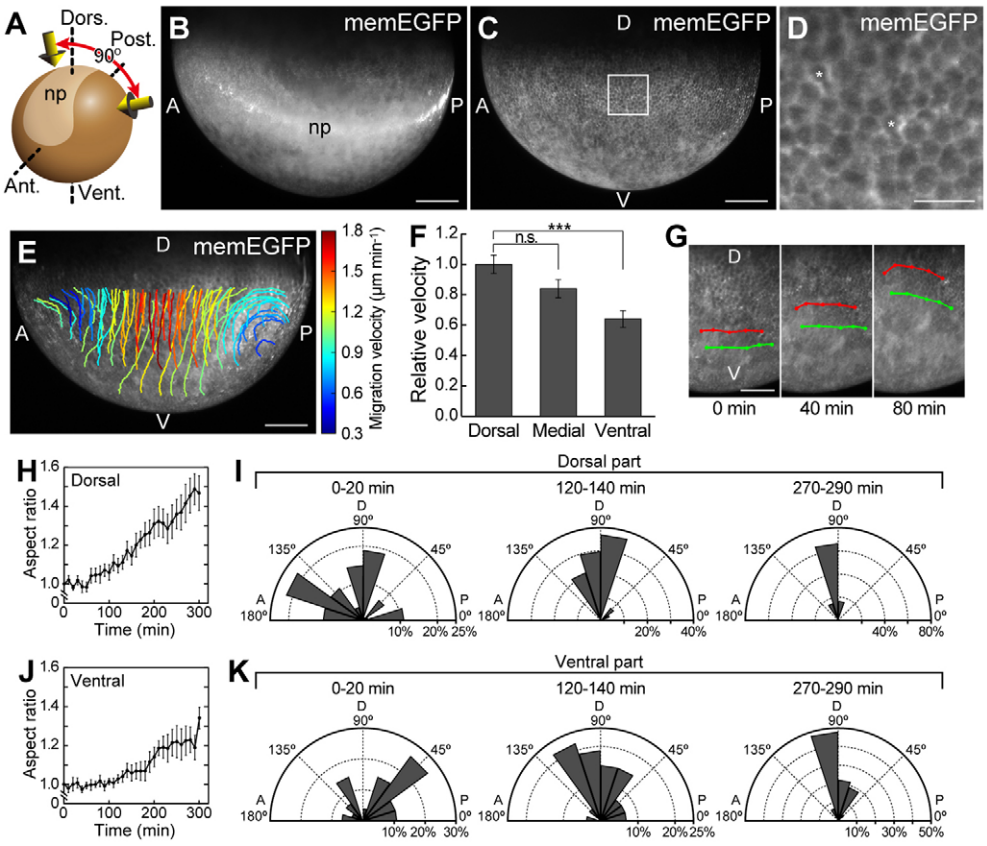

Fig. 1. Dorsally directed stream of non-neural cell movements, fastest in the medial region of the AP axis. (**A**) Schematic diagram of DSLM observation. Early neurula embryos embedded in a DSLM sample capillary were rotated around the AP axis by 90° for dorsal and lateral observation (yellow arrows). np, neural plate. (**B-D**) DSLM observation of NTC in memEGFP-transgenic embryos. Neurula embryos were observed from the dorsal (B) and lateral (C,D) sides. White boxed region in C is magnified in D, in which the individual cells can be recognized by the memEGFP signal and some cells are dividing (asterisks). np, neural plate. (**E**) Migration velocity of the lateral non-neural cells in a memEGFP-transgenic embryo during NTC. The velocity was measured after three-dimensional reconstruction of the image. (**F**) Relative velocity of non-neural ectoderm cells. Lateral views of neurula embryos in DSLM images were equally divided to analyze the velocity of each region. n=3; data are mean±s.e.m.; ***P<0.001, n.s., not significant, t-test. (**G**) Tracking of relative positions of non-neural cells. Positions of the superficial cells in the lateral view of DSLM image were connected by lines (red and green lines) and were tracked during neurulation. (**H-K**) Relative aspect ratio and angles of the major axis of non-neural ectoderm cells. Time-lapse images were used to measure changes of the aspect ratio (H,J) and the angle of the major axis (I,K) in the dorsal (H,I) and ventral (J,K) parts of the non-neural ectoderm. n=9 for each; data are mean±s.e.m. Scale bars: 200 μm in B,C,E; 100 μm in G; 50 μm in D.

same direction, and cells scarcely changed their relative position and intermingled each other along AP axis (n=3 embryos; Fig. 1G), suggesting that cell rearrangement observed as convergent extension in the neural plate is unlikely to occur or it has only limited effect on the non-neural movement (Elul et al., 1997; Rolo et al., 2009). These results suggest that non-neural ectoderm cells are highly motile and move collectively from the ventral to the dorsal side, without remarkable cell rearrangement.

We next examined how this cell movement is controlled, i.e. whether it is intrinsic movement or driven by non-cell autonomous effects. To understand the cellular effects at the morphological level, we examined cell-shape changes in non-neural ectoderm by measuring the aspect ratio of the cells and angles of their longest axes. This revealed that the cells in the medial region along the AP axis became elongated dorsoventrally during NTC, and this tendency was more remarkable on the cells in the dorsal side of the non-neural ectoderm than those in more ventral side (Fig. 1H-K), demonstrating that they were deformed as if stretched along the DV axis. These observations led us to propose that the cell-shape change is due to an external force that stretches the non-neural ectoderm.

The deep-layer cells actively migrate towards the dorsal side

We next asked what caused the dorsal movement and cell-shape change of the non-neural ectoderm. To address this question, we focused on the movement of the deep-layer cells of the non-neural ectoderm. Although the existence of these cells has been known in *Xenopus* (Schroeder, 1970), the observation of their movement in live embryos had hardly been achieved. By injecting the mRNA for *memGFP* into a slightly deeper part of the eight-cell stage embryos, we preferentially labeled the deep-layer cells (Fig. 2A,B). Interestingly, in contrast to the highly epithelialized superficial layer cells, which are polygonal with sharp edges that reflect well-developed cell-cell adhesion, the deep-layer cells showed an amorphous shape extending protrusions (supplementary material Fig. S3). We confirmed that the deep cells lacked apically localized ZO-1 protein, a characteristic structure of epithelial cells (Fig. 2C,D). Importantly, time-lapse observations showed that the deep cells were highly motile towards the dorsal side (Fig. 2E; supplementary material Movie 5). Quantitative analysis of the movements of the deep and superficial layer cells revealed that the deep cells moved

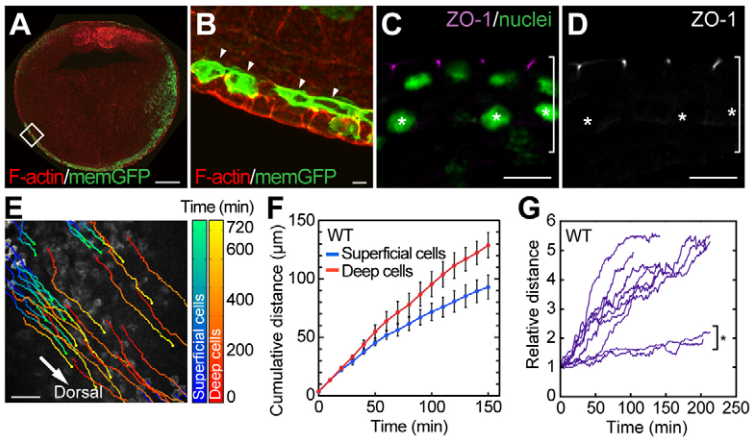

Fig. 2. Deep cells in the non-neural ectoderm actively migrate towards the dorsal side. (**A**,**B**) memGFP labeling of deep-layer cells in non-neural ectoderm. Transverse sections of embryos injected with memGFP into a slightly deep area (A). B is a magnified view of the boxed area in A. Arrowheads indicate deep-layer cells. (**C**,**D**) Localization of ZO-1 in non-neural ectoderm layers. ZO-1 was localized to the apical junction of superficial cells but not in the deep cells (asterisks). Apical side is upwards and basal towards the bottom. White brackets indicate non-neural ectoderm layer. (**E**) Trajectories of superficial and deep cell movements in the non-neural ectoderm of a wild-type embryo. Arrow points towards the dorsal side. (**F**) Cumulative distance from the tracking data of the superficial and deep cells over time. *n*=3; data are mean±s.e.m. (**G**) Relative distance between pairs of non-neural superficial cells and the deep cells beneath them during wild-type NTC. Asterisk and bracket indicate cells in the more ventral side. *n*=9 pairs. Scale bars: 200 μm in A; 100 μm in E; 20 μm in B-D.

faster than the superficial ones (Fig. 2F; superficial, 0.667±0.020 μm min^{-1}; deep, 0.813±0.027 μm min^{-1}). An analysis of pairs of deep and superficial cells that were closely positioned showed that the magnitude of displacement of the deep cell relative to the superficial cell increases as time proceeds (Fig. 2G), although some cells in more ventral areas did not show marked displacement (Fig. 2G, asterisk). These findings suggest that the deep layer cells may play an active role and the superficial cells a passive role in bringing the two neural folds to the midline for NTC.

Dorsal morphogenesis has only a limited effect on the non-neural movement

In a previous study, it was suggested that the tissue movement in the non-neural ectoderm is secondary to the morphogenetic movements in the neural plate (Jacobson and Gordon, 1976). To test this possibility, we inhibited convergent extension and apical constriction, two major morphogenetic movements in the neural plate simultaneously, by a dominant-negative form of Dishevelled (Xdd1) and a morpholino oligonucleotide (MO) against *nectin-2* (nec2-MO), respectively (Wallingford and Harland, 2002; Morita et al., 2010). Embryos co-injected with Xdd1 and nec2-MO into the neural plate region exhibited NT defect phenotype without definitive convergence and apical constriction (closed NT control, *n*=9/9; Xdd1/nec2-MO, *n*=3/12; Fig. 3A-D), indicating an efficient suppression of the neural plate morphogenesis. Then, we observed the non-neural cells in the Xdd1/nec2-MO-injected embryos. Interestingly, we found that dorsally oriented movement of the superficial and deep cells were barely affected (Fig. 3E). The velocity of these cells was slightly slower than those in wild-type embryos (superficial, 0.653±0.019 μm min^{-1}; deep, 0.807±0.027 μm min^{-1}), whereas their relative distance showed a similar profile to that of wild type (Fig. 3F,G). Furthermore, the lateral non-neural cells in the Xdd1/nec2-MO-injected embryos were polarized and elongated along the DV axis, also similarly to those of wild type (Fig. 3H,I). These results suggest that the major morphogenetic movements in the neural plate play a limited role in the non-neural movement and that the non-neural tissue per se generates the significant force for its own morphogenesis.

A dorsal-anteriorly oriented force stretches the non-neural ectoderm

To further test our hypothesis, we employed laser ablation to demonstrate the force on the non-neural ectoderm by cutting the surface of it (Toyama et al., 2008), anticipating that if a stretching force were exerted on the non-neural cells, the gap would expand along the axis of the force. Images of cells just before and after (1.5 seconds) the incision were obtained and merged to measure the displacement (Fig. 4A-C). In most cases, only the superficial cell layer was ablated, leaving the deep layer almost intact (*n*=10/15; Fig. 4D,E). In the cut along the AP axis, we found that the shift of cells on the dorsal side was greater than that on the ventral side at all neurula stages examined (Fig. 4F,G). As the cells in non-neural ectoderm hardly changed their relative positions (Fig. 1G), we assumed that the tension within this tissue is in an equilibrium state; given this, the finding of the dorsally biased displacement suggests that there would be an anisotropic force that allows the cells to move towards the dorsal side as if the deep cells were a moving walk for the superficial ones (red arrows in supplementary material Fig. S4). We also determined the angle of the cell displacement, and found that it was biased towards the anterior side in the lateral area of neurula embryos (Fig. 4H). When another ablation is performed along the DV axis, cells at the anterior and posterior side of the cut shifted markedly towards the anterior and posterior ends, respectively (Fig. 4I-K), suggesting that significant tension is also applied along the AP axis. These results demonstrate that directed tensile force along the dorsal-anterior to ventral-posterior axis is exerted on the superficial layer of the non-neural ectoderm, presumably enabling the global tissue movement.

Dorsal migration of the deep-layer cells is necessary for complete NTC

To prove that the dorsoanterior movement of the non-neural deep cells is the source of the tensile force on the superficial cells and that synchronized cell movements provide the force for complete NTC, we inhibited the cell movement in the non-neural ectoderm. During *Xenopus* neurulation, the three germ layers become clearly separated

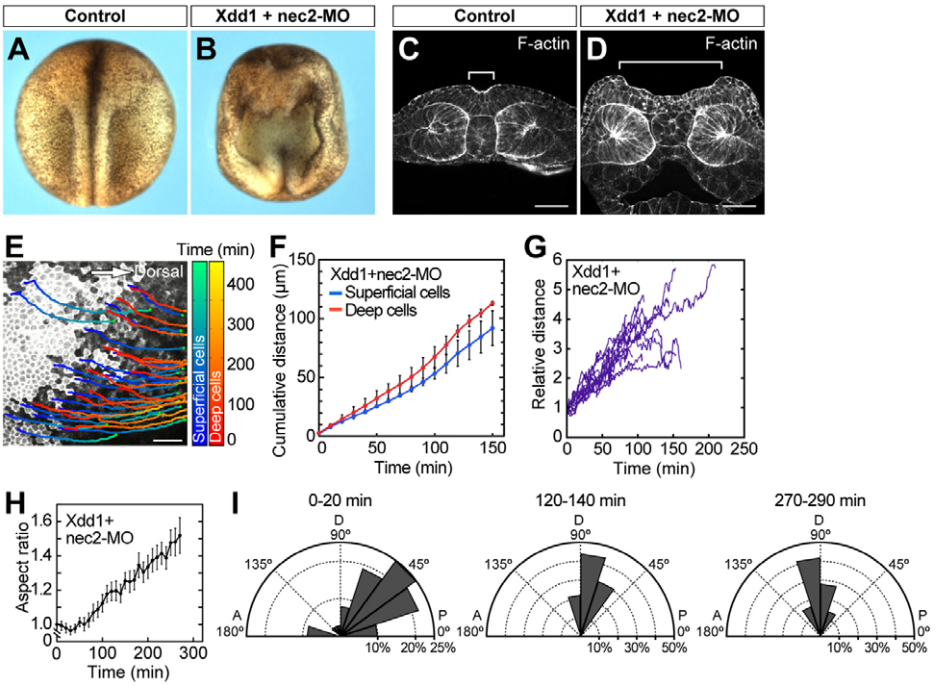

Fig. 3. Dorsal morphogenesis has a limited effect on the non-neural movement. (**A-D**) Phenotype of control and Xdd1/nec2-MO-injected embryos. Embryos were co-injected with Xdd1 and nec2-MO into the dorsal side. When control embryos closed NTs (A), most injected embryos failed to close their NTs (B). Sections of control embryos at mid-neurula stage showed closing NT (C), whereas those of Xdd1/nec2-MO-injected embryos showed widely opened one (D). White brackets indicate neural plate region. (**E**) Trajectories of non-neural cell movement in a Xdd1/nec2-MO-injected embryo. Arrow points towards the dorsal side. (**F**) Cumulative distance of the non-neural superficial and deep cells in Xdd1/nec2-MO-injected embryos. *n*=3; data are mean±s.e.m. (**G**) Relative distance of the non-neural superficial and deep cells in Xdd/nec2-MO-injected embryos. *n*=12 pairs. (**H**,**I**) Relative aspect ratio and angles of the major axis of the non-neural superficial cells in Xdd1/nec2-MO-injected embryos. *n*=12; data are mean±s.e.m. Xdd1 was injected at 2 ng and nec2-MO at 0.5 pmol. Scale bars: 100 μm.

by extracellular matrix (ECM), such as fibronectin (FN) (Davidson et al., 2004), and the cell-ECM adhesion molecule integrin-β1 (Vicente-Manzanares et al., 2009) accumulates at high levels at ectoderm-mesoderm contact site (see supplementary material Fig. S5A-D), indicating that the deep ectoderm cells could attach to and migrate on the ECM via integrins. Previous studies also demonstrated that FN and integrin play important roles in *Xenopus* morphogenetic events, such as gastrulation and NTC (Barreto et al., 2003; Davidson et al., 2006). Therefore, as an attempt to inhibit deep-cell movement, we knocked down *integrin-β1* with its specific MO (Itgβ1-MO; see supplementary material Fig. S5E,F). We injected Itgβ1-MO into the ventral side of the embryos to preferentially inhibit integrin-β1 in the non-neural ectoderm, which we confirmed by co-injecting *memGFP* mRNA as a lineage tracer. At the neurula stage, the neural fold of the MO-injected embryos failed to fuse, leaving a slit along the dorsal midline; this defect was rescued by the co-injection of an integrin-β1 rescue construct (Fig. 5A-D). We further confirmed that this effect of Itgβ1-MO resulted from the knockdown of *integrin-β1* in the non-neural deep cells by transplantation assay, in which we swapped the superficial layers

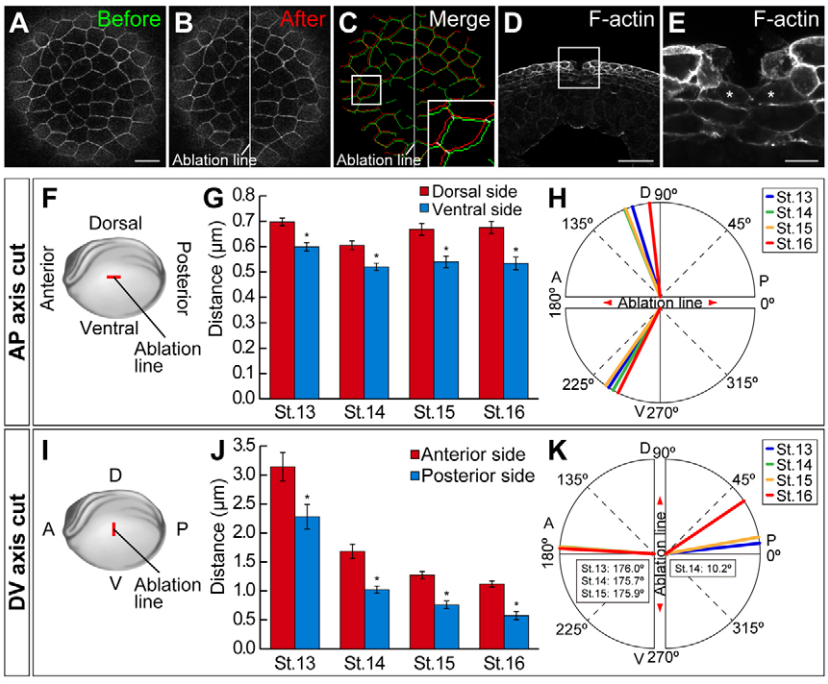

Fig. 4. Dorsoanteriorly directed force on the surface of the non-neural ectoderm. (**A-C**) Laser ablation experiment in non-neural ectoderm. Fluorescent images of a memGFP-injected embryo were taken just before (A) and immediately after (1.5 seconds; B) the incision. These images were merged after image processing, and the displacement of cell vertices between the two time points was measured (C). (**D**,**E**) Sectional views of an embryo fixed immediately after incision. A gap was made on the surface of the embryo without affecting the internal morphologies (D). White boxed region in D is magnified in E. Asterisk indicates deep cells under the ablation site. (**F-H**) Laser ablation along the AP axis. Lateral non-neural ectoderm of neurula embryos was ablated along the AP axis (F, red line). Distance (G) and mean angle (H) of the displacement were measured on the dorsal and ventral sides of the ablation line, respectively, in early (stage 13) to mid- (stage 16) neurula embryos. *n*=27, 23, 16 and 21 (from stage 13 to stage 16); data are mean±s.e.m.; **P*<0.05, *t*-test. (**I-K**) Laser ablation along the DV axis. The lateral side of the neurula was ablated along the DV axis (I, red line). The distance (J) and mean angle (K) were measured on the anterior and posterior side. *n*=6, 5, 7 and 8 (from stage 13 to stage 16); data are mean±s.e.m.; **P*<0.05, *t*-test. Scale bars: 100 μm in D; 20 μm in A,E.

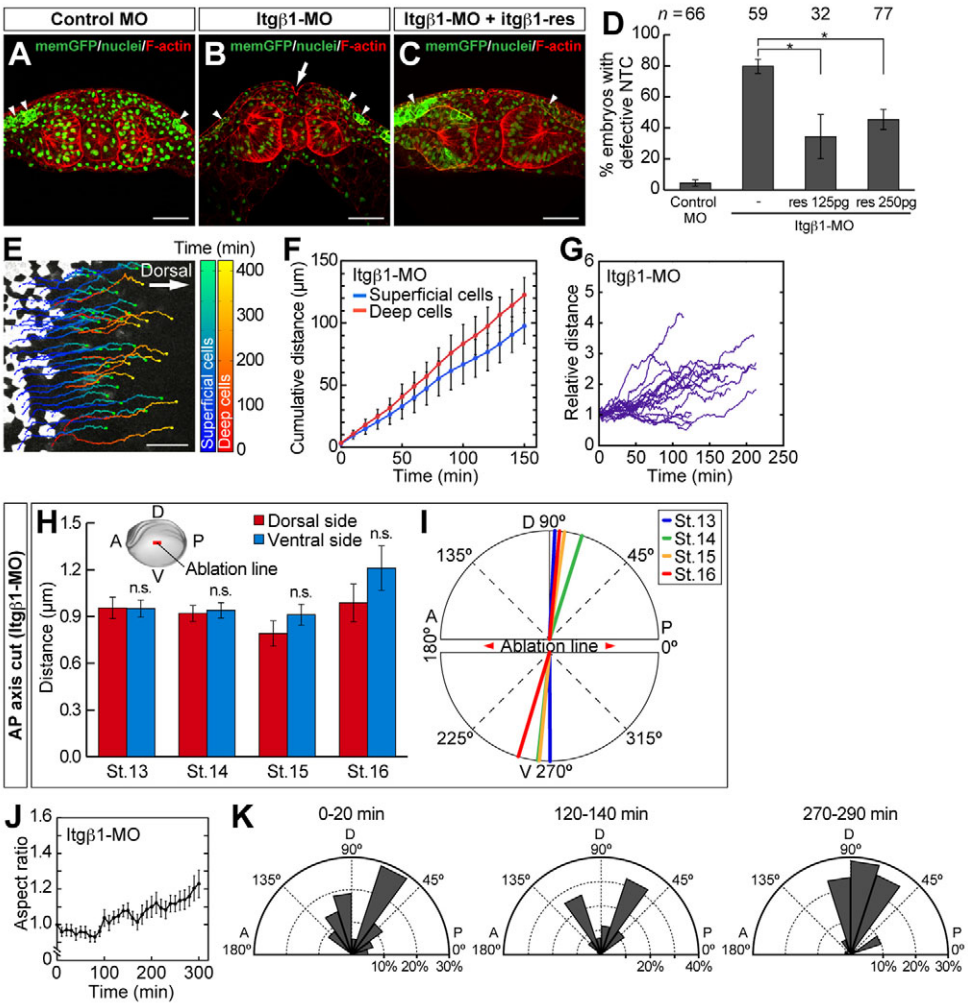

Fig. 5. Inhibition of deep cell movement affects NTC and tension in the superficial cell layer. (**A-C**) Phenotype of *integrin-β1* knockdown in NTC. Transverse sections of late neurula embryos injected with control MO (A), Itgβ1-MO (B) and Itgβ1-MO with rescue mRNA of integrin-β1 (*itgβ1-res*) (C). The NT of Itgβ1-MO-injected embryos failed to completely close (B, arrow). Arrowheads indicate memGFP-positive cells. (**D**) Summary of the MO-injected phenotype. Data are mean±s.e.m. **P*<0.05, *t*-test. (**E**) Trajectories of superficial and deep cell movements in the non-neural ectoderm of Itgβ1-MO-injected embryo. Arrow points towards the dorsal side. (**F**) Cumulative distance from the tracking data of the Itgβ1-MO-injected cells. *n*=3; data are mean±s.e.m. (**G**) Relative distance between pairs of non-neural superficial and deep cells in Itgβ1-MO-injected embryos. *n*=19 pairs. (**H**,**I**) Laser ablation along the AP axis of Itgβ1-MO-injected embryos. Distance (H) and mean angle (I) were measured on the dorsal and ventral sides. *n*=11, 15, 11 and 18 (from stage 13 to stage 16); data are mean±s.e.m.; n.s., not significant, *t*-test. (**J**,**K**) Relative aspect ratio and angles of the major axis of the non-neural superficial cells in Itgβ1-MO-injected embryos. *n*=14; data are mean±s.e.m. *Itgβ1-res* was injected at 250 pg in C and Itgβ1-MO at 10 pmol. Scale bars: 100 μm.

between control and integrin-β1-depleted embryos (see supplementary material Fig. S6A). At the late neurula stage, the embryos with control deep cells normally closed their NTs (closed NT, *n*=9/9), whereas those with integrin-β1-depleted deep cells showed incomplete NTC (*n*=2/7; see supplementary material Fig. S6B-E). These results indicate that the function of integrin-β1 in the non-neural deep cells, but not in the superficial ones, is crucial for complete NTC.

In time-lapse observation, we found that the integrin-β1-depleted cells still moved towards the dorsal side (Fig. 5E; see supplementary material Movie 6). However, quantitative analysis showed that the non-neural cells moved significantly more slowly (superficial: 0.523±0.012 μm min^{-1}; deep: 0.715±0.032 μm min^{-1}) and the changes in distance between superficial and deep cells were smaller than in wild type (Fig. 5F,G). As it is well known that integrins are also involved in cell survival in many species (Bökel and Brown, 2002), we checked the cell death of integrin-β1 morphant using anti-active caspase 3. We found no significant increase in active caspase-3-positive cells (see supplementary material Fig. S5G-K), suggesting that the integrin-β1 inhibition impaired cell movement without affecting cell survival, probably owing to the redundant anti-apoptotic function of other integrin-β subunits expressed in the neurula stages (Ransom et al., 1993).

We next analyzed the tensile force on the non-neural ectoderm of the integrin-β1 morphants. Importantly, after laser ablation, the difference in expansion between the dorsal and ventral sides, and the dorsally biased displacement were no longer observed in the morphants (Fig. 5H,I). In addition, these embryos showed lower aspect ratio and relatively scattered angle of the major axis compared with wild type (Fig. 5J,K), implying that the tension on the superficial cells was reduced as a result of the deficient movement of the non-neural deep cells.

As it was suggested that a change in epithelial cell thickness may drive epidermal cell movement (Brun and Garson, 1983), we examined it in integrin-β1 morphants. In wild type, cell thickness of the non-neural superficial layer decreased during neurulation as reported in other amphibians (Burnside, 1971; Brun and Garson, 1983) (see supplementary material Fig. S5L). Cell thickness in the morphants also decreased with a pattern similar to wild type (see supplementary material Fig. S5L), indicating that Itgβ1-MO does not affect the cell thinning of the non-neural superficial layer. Similarly, it can be evoked that radial intercalation of the non-neural deep cells towards the superficial layer could contribute to the movement of this tissue. During neurulation in *Xenopus*, however, radial intercalation was mostly observed from late neurula stages, in which NT almost closed (Stubbs et al., 2006) (see supplementary material Fig. S5M), suggesting that radial intercalation is unlikely to contribute to the major movement of non-neural ectoderm. Taken together, these results strongly suggest that the active movement of the deep layer cells is indeed the source of tensile force on the superficial cells and that this coordinated movements of non-neural ectoderm contribute to NTC.

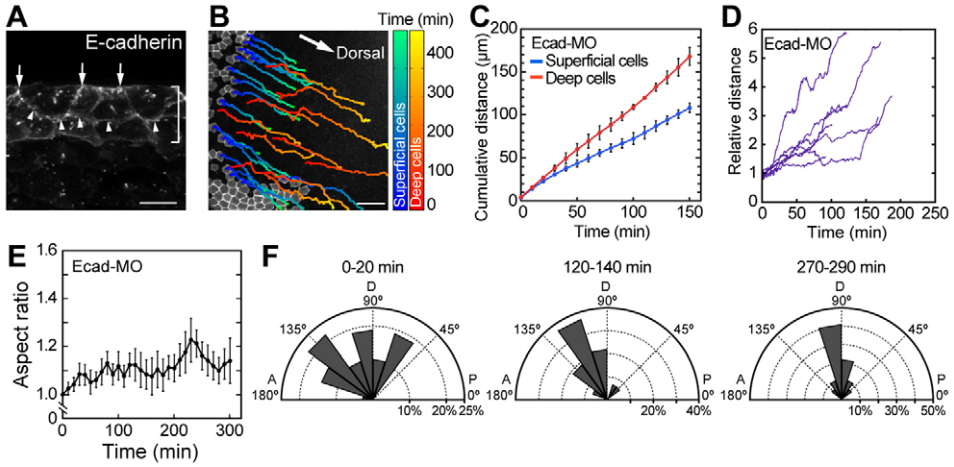

Fig. 6. E-cadherin is required for cooperative cellular movement of the non-neural ectoderm layers. (**A**) Localization of E-cadherin protein in the non-neural ectoderm. E-cadherin is localized not only to the apical junctions (arrows) but also to the border between the superficial and deep cells (arrowheads). White bracket: non-neural ectoderm layer. (**B**) Trajectories of non-neural cell movements in Ecad-MO-injected embryo. Arrow points towards the dorsal side. (**C**) Cumulative distance from the tracking data of the Ecad-MO-injected cells. *n*=3; data are mean±s.e.m. (**D**) Relative distance between pairs of non-neural superficial and deep cells in Ecad-MO-injected embryos. *n*=7 pairs. (**E**,**F**) Relative aspect ratio and angles of the major axis of the non-neural superficial cells in Ecad-MO-injected embryos. Aspect ratio did not increase as it did in wild type (E), whereas the angles of the major axis were somehow polarized (F). *n*=9; data are mean±s.e.m. Ecad-MO was injected at 5.3 pmol (44 ng). Scale bars: 20 μm in A; 100 μm in B.

E-cadherin mediates pulling force between the non-neural deep- and superficial layers

Our findings in the non-neural ectoderm movement suggested that the deep cells might pull the overlying superficial cells, leading them toward the dorsal side. If this were the case, there should be an adhesive interaction between the two layers. In fact, it is known that one of the cell-cell adhesion molecules, E-cadherin, is localized to the border between these layers as well as to the superficial apical junctions in *Xenopus* (Nandadasa et al., 2009) (Fig. 6A) and that knockdown of *E-cadherin* in the non-neural ectoderm results in a significant delay in neurulation (Nandadasa et al., 2009). We then examined whether E-cadherin-mediated cell adhesion is involved in the movement of the non-neural cells using MO (Ecad-MO). We found that, although Ecad-MO-injected non-neural cells moved towards the dorsal side (Fig. 6B), absolute value of velocity of the deep layer and relative distance of both layers were significantly larger than those of wild type (Fig. 6C,D; superficial, 0.759±0.010 μm min^{-1}; deep, 1.208±0.034 μm min^{-1}). However, we found that the aspect ratio of the E-cadherin-depleted non-neural cells did not change drastically during neurulation compared with wild type (Fig. 6E), although the angle of the major axis somehow became polarized (Fig. 6F). These results suggest that detachment of the two layers are enhanced by the loss of E-cadherin, and support our hypothesis that cell-cell interactions between the two layers of non-neural ectoderm would enable the coordinated movement towards the dorsal side that is required for complete NTC.

DISCUSSION

In vertebrate NTC, the cellular mechanisms underlying this dynamic morphogenesis have been well characterized especially in the neural ectoderm, such as convergent extension and apical constriction. For the morphogenesis of the non-neural ectoderm, although some hypotheses were proposed, including cell division, cell rearrangement and cell-shape changes, it has been unclear what drives the movement of this tissue and how it contributes to NTC. Here, we demonstrated the cellular movements of non-neural ectoderm in a whole live embryo, and found that collectively moving deep-layer cells of this tissue contribute to the superficial movement and complete NTC of *Xenopus laevis*.

Present and previous studies showed that cell division is not essential for *Xenopus* NTC. We also attempted to disrupt this oriented cell division by Xdd1, which is known to disrupt the oriented cell division of mesodermal cells in zebrafish (Gong et al., 2004). Unlike the zebrafish mesoderm cells, we could not find randomization of the division plane of the non-neural superficial cells in Xdd1-injected embryos but, rather, the cell division itself was decelerated compared with wild type (data not shown). Moreover, these embryos achieved complete NTC that was indistinguishable from wild type. Therefore, although we were unable to estimate the contribution of ‘oriented’ cell division to NTC, the results further supported the idea that cell division is not essential for NTC.

In contrast to the superficial cells, which form well-organized apical junctions, the deep-layer cells in the non-neural ectoderm exhibited a mesenchyme-like shape with active extension of protrusions, as observed in the deep cells in neural ectoderm (Elul et al., 1997). Their mesenchymal cell-like morphology and the estimation of velocity as being higher than that of the superficial cells support the notion that not superficial cells but the deep cells actively migrate towards the dorsal side. The present and previous studies showed these cell layers are attached each other through E-cadherin (Nandadasa et al., 2009). The fact that disruption of E-cadherin in non-neural ectoderm caused incomplete NTC and the larger difference in the cumulative distance between the superficial and deep cells, namely the decoupling of two layers suggests an important role of the cell-cell adhesion in this coordinated tissue movement. Even though our data imply that the ectodermal deep cells autonomously migrate towards the dorsal side, we cannot rule out the possibility that the movement of these cells might be affected by that of underlying mesoderm cells, which we could not observe because of its opaqueness. To address whether the mesoderm has active roles in this process rather than just being a footing for the epidermal deep layer, current bio-imaging techniques would need to be improved.

To analyze tension in the non-neural superficial cells, we performed laser ablation and demonstrated that cells differently expanded from the cut line in both DV and AP directions. The data also showed that the cell displacements were greater in the AP axis than in the DV axis, implying higher tension along the AP direction. This tension would be generated by convergent extension movements in neural plate and notochord that elongate the embryo anteroposteriorly (Keller, 2002), and a similar tendency was reported in a study of axolotl neurulation (Veldhuis et al., 2005), suggesting that the tissue elongation along the AP axis exerts higher tension on the surface epithelium compared with the DV direction in amphibian neurulation. Similarly, the displacements after ablation along the AP axis in integrin-β1 morphants were higher than that of wild type (Fig. 4G, Fig. 5H). One possibility to explain this observation is that *integrin-β1* knockdown in the deep cells may lead to a reduction of mature focal adhesions of these cells on ECM and make this tissue less stable upon the ablation, whereas the velocity of active migration decreases by the reduction of focal adhesions. How the tension along AP is generated remains to be solved.

In a previous study, it has been reported that integrin-α6, which forms heterodimer with integrin-β1, plays essential role in the neural ectoderm during neurulation (Lallier et al., 1996), intimating a possible function of integrin-β1 in this tissue. By injecting Itgβ1-MO into the dorsal side, we did observe a defective NTC phenotype similar to the one shown in integrin-α6 inhibition (Lallier et al., 1996) (data not shown). However, we did not observe the same phenotype in embryos injected with Itgβ1-MO into the non-neural ectoderm, again suggesting the specificity of Itgβ1-MO effect in the ventral tissue.

Taken together, our present findings reveal a mechanism for the morphogenetic movement of non-neural ectoderm and its contribution to *Xenopus* NTC, and may provide new insight into a general role for coordinated morphogenetic changes in organ formation throughout the organism.

Acknowledgements

We thank Drs K. Okada, K. Tatematsu and H. Igarashi, and Ms. M. Ikeuchi for the laser ablation and discussions; Dr J. B. Wallingford for Xdd1 construct; Drs C. Wylie and S. Nandadasa for Ecad-MO; and the Functional Genomics Facility staff of NIBB for technical assistance. We are grateful to Drs Y. Toyama and T. Matsumoto for helpful discussions, and to Dr C. P. Heisenberg for advice and suggestion on the manuscript.

Funding

This work was supported by KAKENHI [22127007 to N.U.] and by an incentive payment from Daiko Foundation to H.M.

Competing interests statement

The authors declare no competing financial interests.

Supplementary material

Supplementary material available online at
http://dev.biologists.org/lookup/suppl/doi:10.1242/dev.073239/-/DC1

References

Agius, E., Oelgeschlager, M., Wessely, O., Kemp, C. and De Robertis, E. M. (2000). Endodermal Nodal-related signals and mesoderm induction in Xenopus. *Development* **127**, 1173-1183.

Alvarez, I. S. and Schoenwolf, G. C. (1992). Expansion of surface epithelium provides the major extrinsic force for bending of the neural plate. *J. Exp. Zool.* **261**, 340-348.

Amaya, E. and Kroll, K. L. (1999). A method for generating transgenic frog embryos. *Methods Mol. Biol.* **97**, 393-414.

Barreto, G., Reintsch, W., Kaufmann, C. and Dreyer, C. (2003). The function of Xenopus germ cell nuclear factor (xGCNF) in morphogenetic movements during neurulation. *Dev. Biol.* **257**, 329-342.

Bayaa, M., Booth, R. A., Sheng, Y. and Liu, X. J. (2000). The classical progesterone receptor mediates Xenopus oocyte maturation through a nongenomic mechanism. *Proc. Natl. Acad. Sci. USA* **97**, 12607-12612.

Bökel, C. and Brown, N. H. (2002). Integrins in development: moving on, responding to, and sticking to the extracellular matrix. *Dev. Cell* **3**, 311-321.

Brun, R. B. and Garson, J. A. (1983). Neurulation in the Mexican salamander (Ambystoma mexicanum): a drug study and cell shape analysis of the epidermis and the neural plate. *J. Embryol. Exp. Morphol.* **74**, 275-295.

Burnside, B. (1971). Microtubules and microfilaments in newt neuralation. *Dev. Biol.* **26**, 416-441.

Burnside, B. (1973). Microtubules and microfilaments in amphibian neurulation. *Am. Zool.* **13**, 989-1006.

Chung, H. A., Hyodo-Miura, J., Nagamune, T. and Ueno, N. (2005). FGF signal regulates gastrulation cell movements and morphology through its target NRH. *Dev. Biol.* **282**, 95-110.

Colas, J.-F. and Schoenwolf, G. C. (2001). Towards a cellular and molecular understanding of neurulation. *Dev. Dyn.* **221**, 117-145.

Davidson, L. A. and Keller, R. E. (1999). Neural tube closure in Xenopus laevis involves medial migration, directed protrusive activity, cell intercalation and convergent extension. *Development* **126**, 4547-4556.

Davidson, L. A., Keller, R. and DeSimone, D. W. (2004). Assembly and remodeling of the fibrillar fibronectin extracellular matrix during gastrulation and neurulation in Xenopus laevis. *Dev. Dyn.* **231**, 888-895.

Davidson, L. A., Marsden, M., Keller, R. and Desimone, D. W. (2006). Integrin alpha5beta1 and fibronectin regulate polarized cell protrusions required for Xenopus convergence and extension. *Curr. Biol.* **16**, 833-844.

Dent, J. A., Polson, A. G. and Klymkowsky, M. W. (1989). A whole-mount immunocytochemical analysis of the expression of the intermediate filament protein vimentin in Xenopus. *Development* **105**, 61-74.

Elul, T., Koehl, M. A. and Keller, R. (1997). Cellular mechanism underlying neural convergent extension in Xenopus laevis embryos. *Dev. Biol.* **191**, 243-258.

Goda, T., Takagi, C. and Ueno, N. (2009). Xenopus Rnd1 and Rnd3 GTP-binding proteins are expressed under the control of segmentation clock and required for somite formation. *Dev. Dyn.* **238**, 2867-2876.

Gong, Y., Mo, C. and Fraser, S. E. (2004). Planar cell polarity signalling controls cell division orientation during zebrafish gastrulation. *Nature* **430**, 689-693.

Hackett, D. A., Smith, J. L. and Schoenwolf, G. C. (1997). Epidermal ectoderm is required for full elevation and for convergence during bending of the avian neural plate. *Dev. Dyn.* **210**, 397-406.

Hardcastle, Z. and Papalopulu, N. (2000). Distinct effects of XBF-1 in regulating the cell cycle inhibitor p27(XIC1) and imparting a neural fate. *Development* **127**, 1303-1314.

Harland, R. M. (1991). In situ hybridization: an improved whole-mount method for Xenopus embryos. *Methods Cell Biol.* **36**, 685-695.

Harris, W. A. and Hartenstein, V. (1991). Neuronal determination without cell division in Xenopus embryos. *Neuron* **6**, 499-515.

Jacobson, A. G. and Gordon, R. (1976). Changes in the shape of the developing vertebrate nervous system analyzed experimentally, mathematically and by computer simulation. *J. Exp. Zool.* **197**, 191-246.

Jacobson, A. G. and Moury, J. D. (1995). Tissue boundaries and cell behavior during neurulation. *Dev. Biol.* **171**, 98-110.

Keller, P. J., Schmidt, A. D., Wittbrodt, J. and Stelzer, E. H. (2008). Reconstruction of zebrafish early embryonic development by scanned light sheet microscopy. *Science* **322**, 1065-1069.

Keller, R. (2002). Shaping the vertebrate body plan by polarized embryonic cell movements. *Science* **298**, 1950-1954.

Keller, R. E. (1976). Vital dye mapping of the gastrula and neurula of Xenopus laevis. II. Prospective areas and morphogenetic movements of the deep layer. *Dev. Biol.* **51**, 118-137.

Keller, R., Shih, J. and Sater, A. (1992). The cellular basis of the convergence and extension of the Xenopus neural plate. *Dev. Dyn.* **193**, 199-217.

Kroll, K. L. and Amaya, E. (1996). Transgenic Xenopus embryos from sperm nuclear transplantations reveal FGF signaling requirements during gastrulation. *Development* **122**, 3173-3183.

Lallier, T. E., Whittaker, C. A. and DeSimone, D. W. (1996). Integrin alpha 6 expression is required for early nervous system development in Xenopus laevis. *Development* **122**, 2539-2554.

Lee, C., Scherr, H. M. and Wallingford, J. B. (2007). Shroom family proteins regulate gamma-tubulin distribution and microtubule architecture during epithelial cell shape change. *Development* **134**, 1431-1441.

Lee, J. Y. and Harland, R. M. (2010). Endocytosis is required for efficient apical constriction during Xenopus gastrulation. *Curr. Biol.* **20**, 253-258.

Morita, H., Nandadasa, S., Yamamoto, T. S., Terasaka-Iioka, C., Wylie, C. and Ueno, N. (2010). Nectin-2 and N-cadherin interact through extracellular domains and induce apical accumulation of F-actin in apical constriction of Xenopus neural tube morphogenesis. *Development* **137**, 1315-1325.

Nagai, T., Ibata, K., Park, E. S., Kubota, M., Mikoshiba, K. and Miyawaki, A. (2002). A variant of yellow fluorescent protein with fast and efficient maturation for cell-biological applications. *Nat. Biotechnol.* **20**, 87-90.

Nandadasa, S., Tao, Q., Menon, N. R., Heasman, J. and Wylie, C. (2009). N- and E-cadherins in Xenopus are specifically required in the neural and non-neural ectoderm, respectively, for F-actin assembly and morphogenetic movements. *Development* **136**, 1327-1338.
Nieuwkoop, P. D. and Faber, J. (1994). *Normal Table of Xenopus laevis (Daudin)*. New York: Garland.
Nishimura, T. and Takeichi, M. (2008). Shroom3-mediated recruitment of Rho kinases to the apical cell junctions regulates epithelial and neuroepithelial planar remodeling. *Development* **135**, 1493-1502.
Ransom, D. G., Hens, M. D. and DeSimone, D. W. (1993). Integrin expression in early amphibian embryos: cDNA cloning and characterization of Xenopus beta 1, beta 2, beta 3, and beta 6 subunits. *Dev. Biol.* **160**, 265-275.
Roffers-Agarwal, J., Xanthos, J. B., Kragtorp, K. A. and Miller, J. R. (2008). Enabled (Xena) regulates neural plate morphogenesis, apical constriction, and cellular adhesion required for neural tube closure in Xenopus. *Dev. Biol.* **314**, 393-403.
Rolo, A., Skoglund, P. and Keller, R. (2009). Morphogenetic movements driving neural tube closure in Xenopus require myosin IIB. *Dev. Biol.* **327**, 327-338.
Rupp, R. A. and Weintraub, H. (1991). Ubiquitous MyoD transcription at the midblastula transition precedes induction-dependent MyoD expression in presumptive mesoderm of X. laevis. *Cell* **65**, 927-937.
Sater, A. K., Steinhardt, R. A. and Keller, R. (1993). Induction of neuronal differentiation by planar signals in Xenopus embryos. *Dev. Dyn.* **197**, 268-280.
Sausedo, R. A., Smith, J. L. and Schoenwolf, G. C. (1997). Role of nonrandomly oriented cell division in shaping and bending of the neural plate. *J. Comp. Neurol.* **381**, 473-488.
Schoenwolf, G. C. and Alvarez, I. S. (1991). Specification of neurepithelium and surface epithelium in avian transplantation chimeras. *Development* **112**, 713-722.
Schroeder, T. E. (1970). Neurulation in Xenopus laevis. An analysis and model based upon light and electron microscopy. *J. Embryol. Exp. Morphol.* **23**, 427-462.
Smith, J. L. and Schoenwolf, G. C. (1997). Neurulation: coming to closure. *Trends Neurosci.* **20**, 510-517.
Stubbs, J. L., Davidson, L., Keller, R. and Kintner, C. (2006). Radial intercalation of ciliated cells during Xenopus skin development. *Development* **133**, 2507-2515.
Suzuki, A., Shioda, N. and Ueno, N. (1995). Bone morphogenetic protein acts as a ventral mesoderm modifier in early Xenopus embryos. *Dev. Growth Differ.* **37**, 581-588.
Suzuki, M., Hara, Y., Takagi, C., Yamamoto, T. S. and Ueno, N. (2010). MID1 and MID2 are required for Xenopus neural tube closure through the regulation of microtubule organization. *Development* **137**, 2329-2339.
Toyama, Y., Peralta, X. G., Wells, A. R., Kiehart, D. P. and Edwards, G. S. (2008). Apoptotic force and tissue dynamics during Drosophila embryogenesis. *Science* **321**, 1683-1686.
Ubbels, G. A., Hara, K., Koster, C. H. and Kirschner, M. W. (1983). Evidence for a functional role of the cytoskeleton in determination of the dorsoventral axis in Xenopus laevis eggs. *J. Embryol. Exp. Morphol.* **77**, 15-37.
Veldhuis, J. H., Brodland, G. W., Wiebe, C. J. and Bootsma, G. J. (2005). Multiview robotic microscope reveals the in-plane kinematics of amphibian neurulation. *Ann. Biomed. Eng.* **33**, 821-828.
Vicente-Manzanares, M., Choi, C. K. and Horwitz, A. R. (2009). Integrins in cell migration-the actin connection. *J. Cell Sci.* **122**, 199-206.
Wallingford, J. B. (2005). Neural tube closure and neural tube defects: studies in animal models reveal known knowns and known unknowns. *Am. J. Med. Genet. C Semin. Med. Genet.* **135C**, 59-68.
Wallingford, J. B. and Harland, R. M. (2002). Neural tube closure requires Dishevelled-dependent convergent extension of the midline. *Development* **129**, 5815-5825.